Progress In Electromagnetics Research C, Vol. 173, 134–141, 2026

PIER C

(Received 8 June 2026, Accepted 13 August 2026, Scheduled 4 September 2026)

Enhancing Reliability in 6G IoT Networks through Full-Duplex Decode-and-Forward Relaying with Maximum Ratio Transmission

Awfa Aladwani[1,2*] and Tansal Gucluoglu[2]

[1]Computer Center, University of Mosul, Mosul, Iraq
[2]Department of Electronics and Communications Engineering, Faculty of Electrical and Electronics
Yildiz Technical University, Istanbul, Turkey

ABSTRACT: Compared with widely used half-duplex relaying, developing full-duplex (FD) relaying devices enables simultaneous transmission and reception, which can be desirable for spectrally efficient 6G Internet of Things (IoT) networks. To improve the reliability of FD relaying, MRT can be incorporated into an FD-DF relaying architecture, making the resulting scheme practical for diverse applications. In this study, critical performance metrics, such as outage probability, symbol error rate, and channel capacity, were derived for the Nakagami-m fading channel model. Numerical examples from Monte Carlo simulations corroborate the theoretical expressions and demonstrate that MRT can efficiently mitigate residual self-interference while preserving low receiver complexity. These findings provide useful insights for system designers to consider FD-DF relaying with MRT as a practical and effective solution for next-generation wireless ecosystems.

1. INTRODUCTION

The evolution of wireless applications and the increasing number of devices are paving the way for sixth-generation (6G) networks, which will be designed to meet unprecedented demands in capacity, reliability, and scalability [1]. Unlike earlier generations, 6G aims to support an ultra-dense Internet of Things (IoT) ecosystem, where billions of low-power devices coexist with high-throughput applications [2]. Key expectations include massive connectivity, ultra-low latency, high energy efficiency, and simplified architectures capable of handling intense interference and maintaining consistent performance under diverse channel conditions [3]. Cooperative communications via relaying have long been recognized as a cornerstone for enabling coverage extension, improved reliability, increased system capacity, and reduced power consumption [4, 5].

Relay devices have been widely used to connect two wireless links, especially to increase the range and provide diverse paths to base stations. There are two popular relaying approaches: amplify-and-forward (AF) and decode-and-forward (DF) [6, 7]. Although AF relaying has lower computational complexity than DF relaying, DF relaying can provide better performance and may therefore be preferable [8, 9], especially when noise and interference increase. According to 3GPP standardization studies [10], DF can increase cell-edge performance in "long term evolution-advanced" (LTE-A) systems. Recently, DF relaying has been studied for both RF and optical links in [11, 12], where switching between RF and optical channels according to link conditions has been shown to improve overall system performance. Research on relaying has favored half-duplex (HD) relays in practical deployment [4–10]; however, emerging full-duplex (FD) relay devices can further increase the system capacity, as they can transmit and receive at the same time-frequency resource block, which is very valuable due to the enormous increase in the number of wireless devices. Alves et al. [13] compared the performance of FD and HD relaying systems over Rayleigh fading channels. The optimal number of activated device-to-device (D2D) links and mode selection for full-duplex/half-duplex cellular networks were investigated in [14]. Furthermore, the outage performance and power allocation problem of FD-D2D communication were explored in [15]. Chen et al. studied the spectral and energy efficiencies of different FD relaying schemes in [16]. Besides, FD relaying in multiuser systems is considered in [17] for non-orthogonal multiple access (NOMA) and rate-splitting multiple access (RSMA) [18], demonstrating significant performance improvement. The average sum rate and Outage Probability (OP) of RSMA with FD relaying for unmanned air vehicle communication were obtained in [19]. Tani et al. obtained detection probabilities of FD cognitive radio systems in [20]. The outage probability of a cognitive FD-DF relaying system with power constraints was obtained in [21], while Kwon et al. [22] provided the exact OP of an FD-DF relay system over Rayleigh fading channels. Achievable rates were obtained under different power control schemes for the FD-DF relaying system in [23]. The average bit error probability and diversity gain of an FD-DF system were investigated in [24]. Although FD relays attempt to minimize self-interference (SI) at the relay with

* Corresponding author: Awfa Aladwani (awfa.aladwani@uomosul.edu.iq).

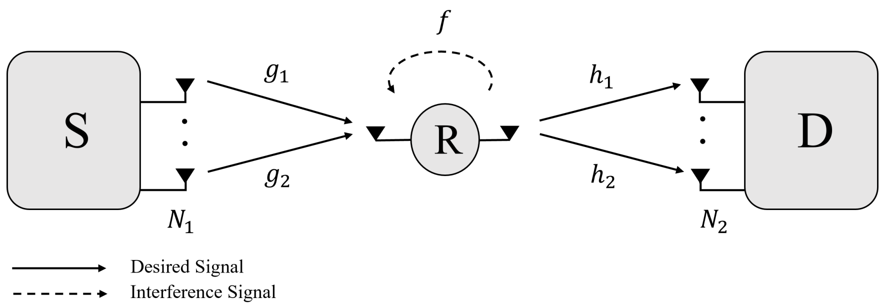

FIGURE 1. Dual-hop maximum-ratio transmission with full-duplex relay.

the help of high electromagnetic isolation, they still experience residual SI [25] because perfect isolation is impractical. Therefore, reliability degradation must be addressed in FD-DF systems to make them appealing for future networks.

Utilizing multiple antennas can improve reliability and capacity depending on the requirements of the wireless application [26]. For example, the performance comparison of multiple antenna systems with half and full-duplex modes over Rayleigh, Rician, and Nakagami-m fading channels was studied in [27]. A practical multi-antenna technique for reducing distortion is maximum ratio transmission (MRT) [28], which increases received signal power and exploits full spatial diversity [29, 30]. Using MRT can still keep receiver's complexity low, which is desirable, especially at the downlink of cellular and WiFi systems, where mobile devices are expected to be small and consume low power. In [3], the spectral efficiency of FD decode-and-forward systems with MRT over Ricean fading channels was investigated. The block error rate of different MIMO schemes containing MRT was studied in [32]. With the advent of conventional MIMO transmissions, we believe that FD decode-and-forward relaying with MRT can be easily adopted for wireless sensor networks and upcoming new technology standards expected to support an enormous number of IoT devices.

In this study, we comprehensively analyze the performance of FD-DF relaying with MRT over Nakagami-m fading channels. In particular, OP, SER, and capacity expressions were derived, and the resulting closed-form expressions were validated through extensive Monte Carlo simulations. Unlike most existing studies, the proposed model explicitly considers residual self-interference and demonstrates that MRT can effectively mitigate its impact while maintaining a low receiver complexity. Moreover, the impacts of self-interference, fading severity, and antenna configuration are evaluated to offer insights for practical system design in ultra-reliable, high-capacity networks. The numerical results confirm that the system achieves significant reliability and capacity gains compared to half-duplex relaying, making FD-DF with MRT a practical and efficient solution for upcoming networks such as 6G IoT and industrial sensor networks.

In the remainder of this paper, Section 2 presents the considered system, and Section 3 provides signal-to-noise ratio (SNR) statistics. Section 4 presents the analysis of performance metrics. Section 5 explains simulation results, and Section 6 summarizes conclusions.

2. SYSTEM DESCRIPTION

Fig. 1 shows the basic system block diagram for FD-DF relaying with MRT. The source device S with N_1 antennas is linked to destination terminal D with N_2 antennas through a single-antenna FD relay. For example, this system can be used when the line-of-sight is blocked because of severe signal distortion, which is realistic in crowded networks in urban areas. The received signal $y_r(n)$ at the relay can be expressed as

$$y_r(n) = \mathbf{g}^T \mathbf{w} x_s(n) + f x_r(n-\tau) + n_r(n), \tag{1}$$

where $x_s(n)$ is the source symbol at time n with unit energy; $\mathbf{g}$ is the $N_1 \times 1$ complex vector with independent identically distributed (i.i.d.) Nakagami-m fading coefficients, which is assumed to be known at both S and R; T is the transpose operator; $\mathbf{w} = \mathbf{g}^*/||\mathbf{g}||$ is the MRT weighting vector,where $*$ is the complex conjugate operator, and $||\mathbf{g}||$ is the Frobenius norm of $\mathbf{g}$; $x_r(n-\tau)$ is the interfering relay symbol sent τ seconds earlier; f is the Nakagami-m distributed SI coefficient between receive and transmit antenna of the relay; and $n_r(n)$ denotes additive white Gaussian noise (AWGN) sample having σ^2 variance and zero mean. For this system, the signal-to-interference plus noise ratio (SINR) at the relay $\gamma_{_R}$ is

$$\gamma_{_R} = \frac{\gamma_g}{\gamma_f + 1}, \tag{2}$$

where $\gamma_g = ||\mathbf{g}||^2/\sigma^2$ is the instantaneous SNR between the source and relay, and $\gamma_f = |f|^2\sigma_{SI}^2/\sigma^2$ is the instantaneous interference-to-noise ratio (INR) at the relay, where σ_{SI}^2 is the SI power. The relay can use the maximum likelihood (ML) detector to obtain the detected symbol $x_r(n)$ as follows

$$x_r(n) = \text{arg} \min_{x_s \epsilon A_x} |y_r(n) - \mathbf{g}^T \mathbf{w} x_s(n)|, \tag{3}$$

where A_x is the set of modulation symbols. Note that, because the relay generates $x_r(n-\tau)$ itself, it can subtract its own known contribution from $y_r(n)$ prior to detection; however, imperfect RF-chain and channel knowledge prevent exact cancellation, leaving the residual self-interference term already captured by γ_R in (2). The detector in (3), therefore, operates on the residual-interference-limited signal after this cancellation step, rather than on the raw received signal in (1). Furthermore, the relay forwards the detected symbol $x_r(n)$ to the destination, as follows: The destination terminal can use the maximum ratio combining (MRC) to obtain the received signal as

$$y_d(n) = \mathbf{v}^T \mathbf{h} x_r(n) + \mathbf{v}\mathbf{n}_d(n), \tag{4}$$

where $\mathbf{h}$ is the $N_2 \times 1$ complex-valued Nakagami-m fading coefficient vector between the relay and destination; $\mathbf{v} = \mathbf{h}^*/||\mathbf{h}||$ is the MRC weight vector where $||\mathbf{h}||$ is the Frobenius norm of $\mathbf{h}$; and $\mathbf{n}_d(n)$ denotes AWGN samples with σ^2 variance and zero mean. The destination can use the ML detector to find the transmitted symbols as

$$x_d(n) = \arg \min_{x_r \epsilon A_x} |y_d(n) - \mathbf{v}^T \mathbf{h} x_r(n)|. \tag{5}$$

The received SNR at the destination can be written as

$$\gamma_h = \frac{||\mathbf{h}||^2}{\sigma^2}. \tag{6}$$

3. SNR STATISTICS

Because fading channel coefficients for all links are Nakagami-m distributed, γ_g, γ_h, and γ_f have gamma distributions with fading parameters m_1, m_2, and m_3, respectively. The probability density function (PDF) of the gamma-distributed γ random variable for N transmit or receive antennas can be expressed as

$$f_\gamma(\gamma) = \frac{m^{mN}\gamma^{mN-1}}{\bar{\gamma}^{mN}\Gamma(mN)} e^{-m\gamma/\bar{\gamma}}. \tag{7}$$

Eq. (7) is a generic gamma PDF; it is specialized below as $f_{\gamma_g}(x)$ with $(m,N) = (m_1,N_1)$ for the source-relay link, $f_{\gamma_h}(x)$ with $(m,N) = (m_2,N_2)$ for the relay-destination link, and $f_{\gamma_f}(x)$ with $(m,N) = (m_3,1)$ for the single-antenna residual self-interference link. The analysis for channels represented as one-sided Gaussian $(m = 1/2)$, Rayleigh $(m = 1)$, and Ricean with K factor $\big(m = (K+1)^2/(2K+1)\big)$ distributions can be readily performed by selecting the fading parameter m accordingly. For SINR at the relay γ_R, the cumulative distribution function (CDF) $F_{\gamma_R}(x)$ can be expressed as

$$F_{\gamma_R}(x) = \Pr(\gamma_R < x), \tag{8}$$

Using γ_R in (2) and corresponding PDFs, (8) can be obtained as follows

$$F_{\gamma_R}(x) = \int_0^\infty \Pr\left(\frac{\gamma_g}{\gamma_f + 1} < x\right) f_{\gamma_f}(\gamma_f) \mathrm{d}\gamma_f \tag{9}$$

$$= \int_0^\infty F_{\gamma_g}\big((\gamma_f+1)x\big) f_{\gamma_f}(\gamma_f) \mathrm{d}\gamma_f \tag{10}$$

$$= \frac{m_3^{m_3}}{\bar{\gamma_f}^{m_3}\Gamma(m_3)\Gamma(m_1N_1)} \times \int_0^\infty \gamma_f^{m_3-1}\gamma\left(m_1N_1, \frac{m_1}{\bar{\gamma_g}}(\gamma_f+1)x\right) e^{-\frac{m_3}{\bar{\gamma_f}}\gamma_f} \mathrm{d}\gamma_f, \tag{11}$$

Using Eqs. (8.352.2), (3.352.3), (0.306), and (1.111) in [33], Eq. (11) can be expressed as

$$F_{\gamma_R}(x) = 1 - \frac{(\frac{m_3}{\bar{\gamma_f}})^{m_3}}{\Gamma(m_3)} e^{-(\frac{m_1}{\bar{\gamma_g}})x} \sum_{n=0}^{m_1N_1-1} \frac{(\frac{m_1 x}{\bar{\gamma_g}})^n}{n!} \times \sum_{k=0}^{n} (k+m_3-1)! \left(\frac{m_3}{\bar{\gamma_f}} + \frac{m_1}{\bar{\gamma_g}}x\right)^{-k-m_3}, \tag{12}$$

where $\Gamma(.,.)$ represents the upper incomplete gamma function [33, 8.350.2]. The CDF of the received SNR at the destination can be obtained as

$$F_{\gamma_h}(x) = 1 - \frac{\Gamma\big(m_2N_2, m_2(\frac{\gamma_h}{\bar{\gamma_h}})\big)}{\Gamma(m_2N_2)}, \tag{13}$$

by using [33, 8.352.7], (13) can be simplified as

$$F_{\gamma_h}(x) = 1 - e^{-m_2\frac{x}{\bar{\gamma_h}}} \sum_{l=0}^{m_2N_2-1} \left(m_2 \frac{x}{\bar{\gamma_h}}\right)^l \frac{1}{l!}. \tag{14}$$

Moreover, the PDF of the first hop SNR can be calculated as

$$f_{\gamma_R}(x) = \int_0^\infty (1+x) f_{\gamma_g}((x+1)\gamma) f_{\gamma_f}(x) \mathrm{d}x, \tag{15}$$

then,

$$f_{\gamma_R}(\gamma) = \frac{(\frac{m_1}{\bar{\gamma_g}})^{m_1N_1}(\frac{m_3}{\bar{\gamma_f}})^{m_3}}{\Gamma(m_1N_1)\Gamma(m_3)} e^{-\frac{m_1}{\bar{\gamma_g}}x}\gamma^{m_1N_1-1} \times \int_0^\infty (x+1)(x+1)^{m_1N_1-1} x^{m_1N_1-1} e^{-\frac{m_1}{\bar{\gamma_g}}\gamma + \frac{m_3}{\bar{\gamma_f}}x} \mathrm{d}x. \tag{16}$$

After some mathematical manipulations, the PDF of the first hop SNR can be obtained as

$$f_{\gamma_R}(\gamma) = \frac{(\frac{m_1}{\bar{\gamma_g}})^{m_1N_1}(\frac{m_3}{\bar{\gamma_f}})^{m_3}}{\Gamma(m_1N_1)\Gamma(m_3)} \gamma^{m_1N_1-1} e^{-\frac{m_1}{\bar{\gamma_g}}\gamma} \times \sum_{n=0}^{m_1N_1} \frac{\binom{m_1N_1}{n}\Gamma(n+m_3)}{(\frac{m_1}{\bar{\gamma_g}}\gamma + \frac{m_3}{\bar{\gamma_f}})^{n+m_3}}. \tag{17}$$

Similar to the above equation, the PDF of the second hop SNR can be given as

$$f_{\gamma_h}(\gamma) = \frac{(\frac{m_2}{\bar{\gamma_h}})^{m_2N_2}}{\Gamma(m_2N_2)} \gamma^{m_2N_2-1} e^{-\frac{m_2}{\bar{\gamma_h}}\gamma}. \tag{18}$$

4. PERFORMANCE ANALYSIS

This section presents an analytical evaluation of the performance metrics of the proposed system. First, closed-form expressions for the outage probability are derived, followed by a detailed symbol error rate analysis. Finally, the ergodic capacity under Nakagami-m fading is determined. These metrics provide a complete picture of the reliability and capability of the FD-DF-MRT system.

4.1. Outage Probability

In this subsection, the OP's analytical expression over the Nakagami-m channel is derived using the SNR CDF. The OP of the dual-hop system can be defined as the probability that at least one of γ_R and γ_h falls below a predefined threshold γ_{th}. Thus, the OP can be written as

$$P_{out} = 1 - \left(Pr(\gamma_R > \gamma_{th})Pr(\gamma_h > \gamma_{th})\right). \tag{19}$$

$\gamma_{th} = 2^{R_0} - 1$ where R_0 denotes the bits per channel use (BPCU). Assuming $R_0 = 1$ BPCU, threshold SNR becomes $\gamma_{th} = 2^1 - 1 = 1$ (linear), i.e., $\gamma_{th} = 0$ dB. Using the derived CDF expressions, OP can be expressed as

$$P_{out} = 1 - \left(\left(1 - F_{\gamma_R}(\gamma_{th})\right)\left(1 - F_{\gamma_h}(\gamma_{th})\right)\right). \tag{20}$$

Substituting Eqs. (12) and (14) into Eq. (20), the final OP can be obtained as follows

$$\begin{aligned} P_{out} = 1 - e^{-m_2\frac{\gamma_{th}}{\bar{\gamma_h}}} \sum_{l=0}^{m_2N_2-1}\left(m_2\frac{\gamma_{th}}{\bar{\gamma_h}}\right)^l \frac{1}{l!} \\ \times \frac{(\frac{m_3}{\bar{\gamma_f}})^{m_3}}{\Gamma(m_3)} e^{-(\frac{m_1}{\bar{\gamma_g}})\gamma_{th}} \sum_{n=0}^{m_1N_1-1} \frac{(\frac{m_1\gamma_{th}}{\bar{\gamma_g}})^n}{n!} \\ \times \sum_{k=0}^{n}(k+m_3-1)!\left(\frac{m_3}{\bar{\gamma_f}} + \frac{m_1}{\bar{\gamma_g}}\gamma_{th}\right)^{-k-m_3}. \end{aligned} \tag{21}$$

4.2. Symbol Error Rate

In order to get the system's error performance, the first- and second-hop SERs are derived separately below (denoted as P_{e1} and P_{e2}) and combined into the end-to-end SER in (30), and the SER can be found by

$$P_{e1} = \int_0^\infty P_e(e|\gamma_R) f_{\gamma_R} d\gamma, \tag{22}$$

where $P_e(e|\gamma_R)$ denotes the symbol error probability conditioned on the instantaneous SINR γ_R and is given as

$$P_e(e|\gamma_R) = \frac{\Gamma(b, a\gamma_R)}{2\Gamma(b)}, \tag{23}$$

which can be expressed in the following form by using Wolfram Mathematica [34, Eq. (06.06.26.0005.01)],

$$P_e(e|\gamma_R) = \frac{1}{2\Gamma(b)} G_{1,2}^{2,0}(a\gamma_R|_{0,b}^{1}). \tag{24}$$

where a and b are modulation-dependent constants of the standard incomplete-gamma SER representation. For example, $a = \sin 2(\pi/M)$, $b = 1/2$ for M-PSK, and $a = 1$, $b = 1/2$ for BPSK, selected according to the modulation format used in Section 5. To this end

$$\begin{aligned} P_{e1} = \frac{(\frac{m_1}{\bar{\gamma_g}})^{m_1N_1}(\frac{m_3}{\bar{\gamma_f}})^{m_3}}{2\Gamma(b)\Gamma(m_1N_1)\Gamma(m_3)} \sum_{m_1N_1}^{n=0}\binom{m_1N_1}{n} \\ \times\Gamma(n+m_3)\int_0^\infty \gamma^{m_1N_1-1}G_{1,2}^{2,0}(a\gamma|_{0,b}^{1}) \\ \times e^{-\frac{m_1}{\bar{\gamma_g}}\gamma}\left(\frac{m_1}{\bar{\gamma_g}}\gamma + \frac{m_3}{\bar{\gamma_f}}\right)^{-(n+m_3)} d\gamma. \end{aligned} \tag{25}$$

symbol error probability of the first hop is obtained as follows

$$\begin{aligned} P_{e1} = \frac{a^{-m_1N_1}(\frac{m_1}{\bar{\gamma_g}})^{m_1N_1}(\frac{m_3}{\bar{\gamma_f}})^{m_3}}{2\Gamma(b)\Gamma(m_1N_1)\Gamma(m_3)} \\ \times\sum_{m_1N_1}^{n=0}\binom{m_1N_1}{n}\left(\frac{m_3}{\bar{\gamma_f}}\right)^{-n-m_3} \\ \times G_{21:01:11}^{02:10:11}\left(\begin{matrix}\frac{m_1}{\alpha\gamma_g} \\ \frac{m_1\gamma_f}{\alpha m_3\gamma_g}\end{matrix}\middle|\begin{matrix}1-m_1N_1,1-m_1N_1-b;;1-n-m_3 \\ 1-m_1N_1-1;0;0\end{matrix}\right). \end{aligned} \tag{26}$$

The symbol error probability of the second hop can be obtained using the following equation

$$P_{e2} = \int_0^\infty P_e(e|\gamma_h) f_{\gamma_h}(\gamma) d\gamma. \tag{27}$$

Thus,

$$\begin{aligned} P_{e2} = \frac{(\frac{m_2}{\bar{\gamma_h}})^{m_2N_2}}{2\Gamma(b)\Gamma(m_2N_2)} \\ \int_0^\infty \gamma^{m_2N_2-1}e^{-\frac{m_2}{\bar{\gamma_h}}\gamma}G_{1,2}^{2,0}\left(a\gamma\middle|_{0,b}^{1}\right)d\gamma. \end{aligned} \tag{28}$$

After some mathematical manipulations, the symbol error probability of the second hop can be obtained as

$$P_{e2} = \frac{a^{-m_2N_2}(\frac{m_2}{\bar{\gamma_h}})^{m_2N_2}}{2\Gamma(b)\Gamma(m_2N_2)} G_{2,2}^{1,2}\left(\frac{m_2}{a\bar{\gamma_h}}\middle|_{0,1-m_2N_2-1}^{1-m_2N_2,1-m_2N_2-b}\right). \tag{29}$$

To this end, the system SER performance metric of the two hops can be obtained by [29]

$$P_{e2e} = P_{e1} + P_{e2} - 2\left(P_{e1}\, P_{e2}\right), \tag{30}$$

4.3. Capacity Analysis

The maximum ergodic capacity for the end-to-end system is

$$C_{e2e} = \min(C_1, C_2), \tag{31}$$

where C_1 and C_2 are ergodic capacities of the first and second hops, respectively. The ergodic capacity of the fading channel can be expressed as follows

$$C_i = \int_0^\infty \log_2(1+\gamma) f_{\gamma_R}(\gamma) d\gamma. \tag{32}$$

the ergodic capacity of the first hop is

$$C_1 = \int_0^\infty \log_2(1+\gamma)\left[\frac{(\frac{m_1}{\bar{\gamma}_g})^{m_1N_1}(\frac{m_3}{\bar{\gamma}_f})^{m_3}}{\Gamma(m_1N_1)\Gamma(m_3)}\gamma^{m_1N_1-1}\right.$$
$$\left.\times e^{-(\frac{m_1}{\bar{\gamma}_g})\gamma}\sum_{n=0}^{m_1N_1}\frac{\binom{m_1N_1}{n}\Gamma n+m_3}{(\frac{m_1}{\bar{\gamma}_g}\gamma+\frac{m_3}{\bar{\gamma}_f})^{n+m_3}}\right]d\gamma. \quad (33)$$

Using [35, Eq. (7)], Eq. (33) can be obtained as follows

$$C_1 = \frac{\log_2 e\left(\frac{m_1}{\bar{\gamma}_g}\right)^{m_1N_1}\left(\frac{m_3}{\bar{\gamma}_f}\right)^{m_3}}{\Gamma(m_1N_1)\Gamma(m_3)}$$
$$\times\sum_{n=0}^{m_1N_1}\binom{m_1N_1}{n}\left(\frac{m_3}{\bar{\gamma}_f}\right)^{-(n+m_3)}$$
$$\times\int_0^\infty \gamma^{m_1N_1-1}G_{1,0}^{0,1}\left(\frac{m_1\gamma}{\bar{\gamma}_g}\,\middle|\,0\right)$$
$$\times G_{1,1}^{1,1}\left(\frac{m_1\bar{\gamma}_f}{m_3\bar{\gamma}_g}\gamma\,\middle|\,\begin{matrix}1-n-m_3\\0\end{matrix}\right)$$
$$\times G_{2,2}^{1,2}\left(\gamma\,\middle|\,\begin{matrix}1,1\\1,0\end{matrix}\right)d\gamma, \quad (34)$$

If the expression in the integral term is called I_1 and by using [36, Eq. (07.34.21.0081.01)], I_1 can be obtained as follows

$$I_1 = \left(\frac{m_1}{\bar{\gamma}_g}\right)^{-m_1N_1}$$
$$\times G_{1,0:1,1:2,2}^{0,1:1,1:1,2}\left(\begin{matrix}\frac{\bar{\gamma}_g}{m_1}\\\frac{\bar{\gamma}_f}{m_3}\end{matrix}\,\middle|\,\begin{matrix}-;0;1,0\\1-m_1N_1;1-m_3;1,1\end{matrix}\right), \quad (35)$$

after some mathematical manipulations, C_1 can be obtained as

$$C_1 = \frac{\log_2(e)}{\Gamma(m_1N_1)\Gamma(m_3)}\sum_{n=0}^{m_1N_1}\binom{m_1N_1}{n}\left(\frac{m_3}{\bar{\gamma}_f}\right)^{-n}$$
$$\times G_{1,0:1,1:2,2}^{0,1:1,1:1,2}\left(\begin{matrix}\frac{\bar{\gamma}_g}{m_1}\\\frac{\bar{\gamma}_f}{m_3}\end{matrix}\,\middle|\,\begin{matrix}-;0;1,0\\1-m_1N_1;1-m_3;1,1\end{matrix}\right). \quad (36)$$

Similarly, the ergodic capacity C_2 of the R-D hop can be calculated as follows

$$C_2 = \int_0^\infty \log_2(1+\gamma)f_{\gamma_h}(\gamma)d\gamma, \quad (37)$$

Using the PDF expression in (18), C_2 can be obtained as

$$C_2 = \frac{\log_2(e)\left(\frac{m_2}{\bar{\gamma}_h}\right)^{m_2N_2}}{\Gamma(m_2N_2)}$$
$$\times\int_0^\infty \gamma^{m_2N_2-1}G_{2,2}^{1,2}\left(\gamma\,\middle|\,\begin{matrix}1,1\\1,0\end{matrix}\right)G_{0,1}^{1,0}\left(\frac{m_2}{\bar{\gamma}_h}\gamma\,\middle|\,\begin{matrix}-\\0\end{matrix}\right)d\gamma. \quad (38)$$

The expression in the above integral can be simplified using [36, Eq. (07.34.21.0011.01)]; then, C_2 can be expressed as

$$C_2 = \frac{\log_2(e)}{\Gamma(m_2N_2)}G_{3,2}^{1,3}\left(\frac{\bar{\gamma}_h}{m_2}\,\middle|\,\begin{matrix}1,1,1-m_2N_2\\1,0\end{matrix}\right) \quad (39)$$

5. SIMULATION RESULTS

OP, SER, and capacity results obtained by Monte Carlo simulations are demonstrated in this section to corroborate our analytical expressions and gain insight into the behavior of the studied system. In the OP plots, the power of the SI channel is assumed to be $\sigma_{SI}^2 = 0.1$. Similar to [16], the SNR threshold is selected by assuming BPCU= 1, which gives $\gamma_{th} = 2^1 - 1 = 1$ (linear scale), i.e., $\gamma_{th} = 0$ dB. For both links before and after the FD-DF relays, the SNR values are the same in all figures, in which the numerical results match perfectly with the closed-form theoretical findings.

Figure 2 illustrates the impact of the number of antennas on OP performance when fading parameters are the same for all links. Obviously, using more antennas results in improved OP. For example, at 20 dB SNR, having four antennas compared to two decreases the OP from 10^{-3} to 10^{-7}, showing the effectiveness of MRT. When the power of SI increases, the received SINR at the relay decreases, as can be seen from Eq. (2); thus, the OP drops to a certain level and remains constant, for example, 10^{-5} for $N_1 = N_2 = 3$. For comparison, $\gamma_{th} = 2^{2R_0} - 1 = 3$ (4.77 dB) is used for half-duplex (HD) curves in Fig. 2 to account for the doubled target rate required by the two time slots that HD needs per transmission, while FD curves use $\gamma_{th} = 2^{R_0} - 1 = 1$ (0 dB). As can be seen in the figure, when the BPCU is assumed to be 1 for the HD and FD modes, the FD mode can perform better than the HD at low SNRs, showing that the adverse effects of the SI become smaller. It can be deduced that when SNR increases, the SI degrades performance more; hence, MRT becomes quite helpful without increasing reception complexity. When $N_1 = N_2 = 4$ antennas are used, only 6 dB SNR is sufficient to achieve OP = 10^{-5}, which is essential to satisfy the requirements of highly demanding service availability rates, such as 99.999% of cellular networks.

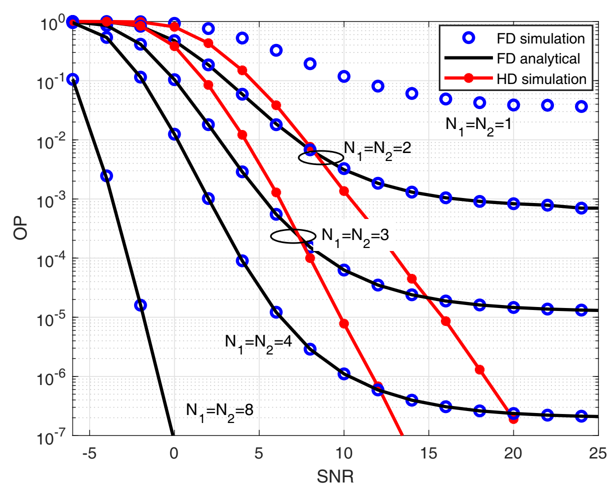

FIGURE 2. Outage probability when fading parameters $m_1 = m_2 = m_3 = 2$, $\gamma_{th} = 0$ dB for FD and 4.77 dB for HD.

Figure 3 illustrates the effect of the fading severity parameter on OP performance. When the fading parameter m increases, OP decreases. When $m_1 = m_2 = m_3 = 1$, channel coefficients at all links become Rayleigh-distributed, in which the

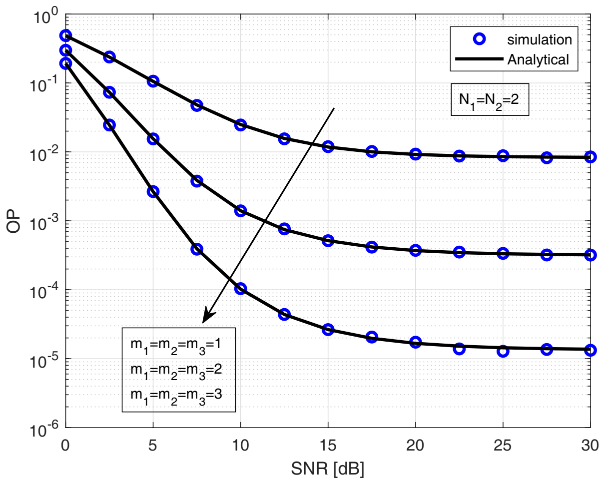

FIGURE 3. Outage probability when number of antennas $N_1 = N_2 = 2$ and $\gamma_{th} = 0$ dB.

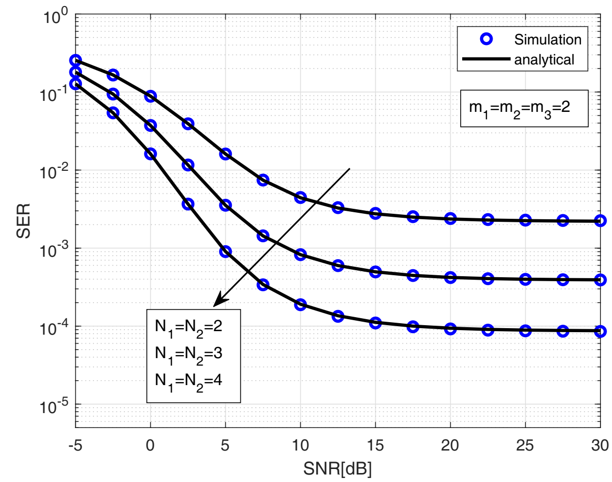

FIGURE 5. Symbol error rate when fading parameters $m_1 = m_2 = m_3 = 2$.

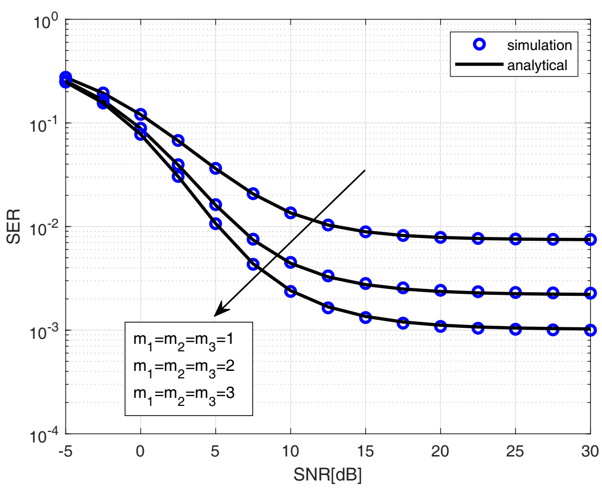

FIGURE 4. Symbol error rate when antenna numbers $N_1 = N_2 = 2$.

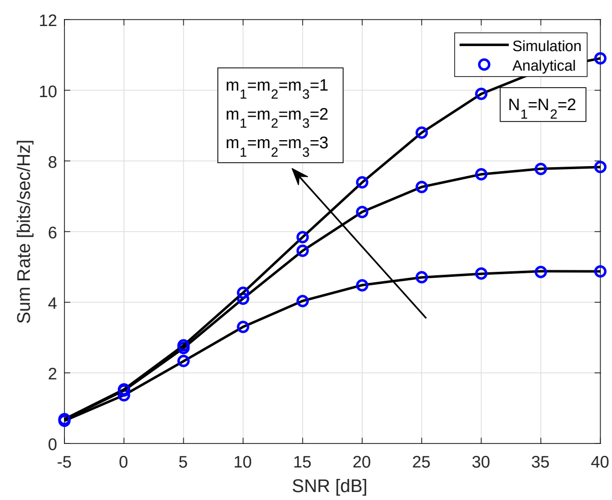

FIGURE 6. Capacity when fading parameters when $N_1 = N_2 = 2$.

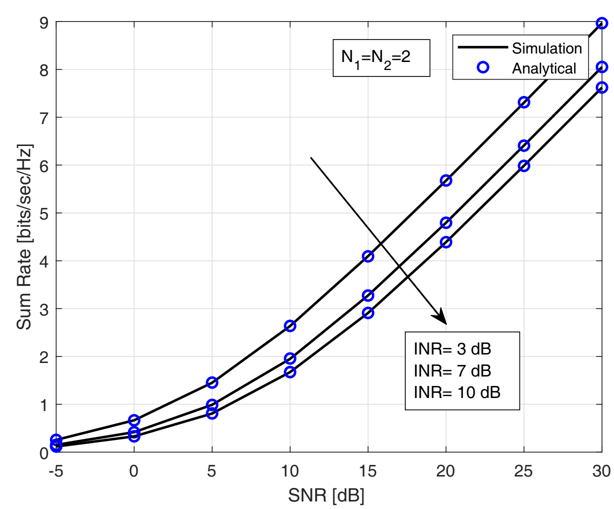

FIGURE 7. Capacity when number of antennas $N_1 = N_2 = 2$.

OP becomes fixed at approximately the 10^{-2} level, which may not be sufficient for high quality of service, and it would be necessary to allocate more antennas for that link. As can be seen in the figure, when $m_1 = m_2 = m_3 = 3$, the OP is 10^{-4} at 10 dB SNR; thus, base stations would allocate few antennas if wireless links do not experience harsh fading.

Figure 4 shows the effect of the fading severity parameter on SER performance. As expected, if the fading parameter increases, the SER decreases. As shown in the figure, when $m_1 = m_2 = m_3 = 3$ and $N_1 = N_2 = 2$ the SER is 10^{-3} at 20 dB SNR.

Figure 5 illustrates the symbol error probability performance when Nakagami-m channel parameters are $m_1 = m_2 = m_3 = 2$. The analytical results fit the simulated results for all cases. As can be seen in the figure, if the number of antennas is increased, the SER decreases. For $N_1 = N_2 = 4$, the SER reaches the 10^{-4} when the SNR exceeds 15 dB.

In Fig. 6, with the number of source and destination antennas $N_1 = N_2 = 2$, a change in ergodic capacity is observed according to the fading severity parameter. Since the channel is one of the factors that significantly affects the ergodic capacity, as can be seen in the figure, if the fading parameters are increased, the capacity also increases. Although the same data rate is obtained in the low-SNR region, a difference arises at high SNRs. At 30 dB SNR, the sum data rate is 5 bits/sec/Hz when $m_1 = m_2 = 1$, and the sum data rate is 8 bits/sec/Hz when $m_1 = m_2 = m_3 = 2$.

Figure 7 shows the effect of changing the INR of the self-interference channel on the ergodic capacity. When the INR and SNR are 3 and 15 dB, respectively, the capacity of the system model is 4 bits/sec/Hz. If the INR increases to 10 dB, the capacity decreases to 3 bit/sec/Hz.

6. CONCLUSIONS

In this study, closed-form expressions for SINR statistics, OP, SER, and ergodic capacity for FD-DF dual-hop relaying with MRT over Nakagami-m fading channels were derived and validated. The results show that although residual self-interference is unavoidable in FD relaying, its impact can be effectively mitigated by MRT without increasing receiver complexity. The numerical results further demonstrate that the proposed scheme remains robust under severe fading, offering improved reliability without added complexity when more antennas are employed. Compared to half-duplex transmission, FD relaying provides clear performance gains, particularly at low SNR conditions. These features make FD-DF with MRT a practical solution for 6G and IoT networks, where ultra-reliability, spectral efficiency, and scalability are critical.

REFERENCES

[1] Yang, N. and A. Shafie, "Terahertz communications for massive connectivity and security in 6G and beyond era," *IEEE Communications Magazine*, Vol. 62, No. 2, 72–78, Feb. 2024.

[2] Adhikari, B., M. Jaseemuddin, and A. Anpalagan, "Resource allocation for co-existence of eMBB and URLLC services in 6G wireless networks: A survey," *IEEE Access*, Vol. 12, 552–581, 2024.

[3] Khan, N., S. Coleri, A. Abdallah, A. Celik, and A. M. Eltawil, "Explainable and robust artificial intelligence for trustworthy resource management in 6G networks," *IEEE Communications Magazine*, Vol. 62, No. 4, 50–56, Apr. 2024.

[4] Chakrabarti, A., A. Sabharwal, and B. Aazhang, "Cooperative communications," in *Cooperation in Wireless Networks: Principles and Applications*, 29–68, Springer, Dordrecht, 2006.

[5] Sendonaris, A., E. Erkip, and B. Aazhang, "User cooperation diversity. Part II. Implementation aspects and performance analysis," *IEEE Transactions on Communications*, Vol. 51, No. 11, 1939–1948, Nov. 2003.

[6] Laneman, J. N., D. N. C. Tse, and G. W. Wornell, "Cooperative diversity in wireless networks: Efficient protocols and outage behavior," *IEEE Transactions on Information Theory*, Vol. 50, No. 12, 3062–3080, Dec. 2004.

[7] Nosratinia, A., T. E. Hunter, and A. Hedayat, "Cooperative communication in wireless networks," *IEEE Communications Magazine*, Vol. 42, No. 10, 74–80, Oct. 2004.

[8] Boujemâa, H., "Static hybrid amplify and forward (AF) and decode and forward (DF) relaying for cooperative systems," *Physical Communication*, Vol. 4, No. 3, 196–205, 2011.

[9] Stosic, J. and Z. Hadzi-Velkov, "Performance analysis of dual-hop MIMO systems," in *International Conference on ICT Innovations*, 123–132, Springer, Berlin, Heidelberg, 2010.

[10] Nokia Siemens Networks, "Cell edge performance for amplify-and-forward vs. decode-and-forward relays," 3GPP TDoc R1-090732, Athens, Greece, 2009.

[11] Zhang, Z., Q. Sun, M. López-Benítez, X. Chen, and J. Zhang, "Performance analysis of dual-hop RF/FSO relaying systems with imperfect CSI," *IEEE Transactions on Vehicular Technology*, Vol. 71, No. 5, 4965–4976, May 2022.

[12] Lou, Y., R. Sun, J. Cheng, D. Nie, and G. Qiao, "Secrecy outage analysis of two-hop decode-and-forward mixed RF/UWOC systems," *IEEE Communications Letters*, Vol. 26, No. 5, 989–993, May 2022.

[13] Alves, H., R. D. Souza, and G. Fraidenraich, "Outage, throughput and energy efficiency analysis of some half and full duplex cooperative relaying schemes," *Transactions on Emerging Telecommunications Technologies*, Vol. 25, No. 11, 1114–1125, Nov. 2014.

[14] Xiao, Z., J. Sun, and X. Sun, "Analysis of the number of activated links and mode selection for full-duplex/half-duplex D2D-aided underlaying cellular networks," *IEICE Transactions on Communications*, Vol. E108-B, No. 7, 761–767, Jul. 2025.

[15] Dang, S., G. Chen, and J. P. Coon, "Outage performance analysis of full-duplex relay-assisted device-to-device systems in uplink cellular networks," *IEEE Transactions on Vehicular Technology*, Vol. 66, No. 5, 4506–4510, May 2017.

[16] Chen, Z., T. Q. S. Quek, and Y.-C. Liang, "Spectral efficiency and relay energy efficiency of full-duplex relay channel," *IEEE Transactions on Wireless Communications*, Vol. 16, No. 5, 3162–3175, May 2017.

[17] Salem, A., K.-K. Wong, C.-B. Chae, and Y. Zhang, "STAR-RIS assisted full-duplex NOMA communication networks," *IEEE Transactions on Wireless Communications*, Vol. 24, No. 3, 2467–2482, Mar. 2025.

[18] Dinh, C. H., X. N. Pham, H. L. T. Thanh, D. T. Tran, and B. C. Nguyen, "Transmit antenna selection for full-duplex relay millimeter-wave communications employing rate-splitting multiple access," *International Journal of Communication Systems*, Vol. 38, No. 3, e6113, 2025.

[19] Singh, S. K., K. Agrawal, K. Singh, B. Clerckx, and C.-P. Li, "RSMA for hybrid RIS-UAV-aided full-duplex communications with finite blocklength codes under imperfect SIC," *IEEE Transactions on Wireless Communications*, Vol. 22, No. 9, 5957–5975, Sep. 2023.

[20] Tani, A., D. Marabissi, and R. Fantacci, "Efficient real-time whitening for blind eigenvalue-based detection in mmWave full duplex cognitive radio," *IEEE Transactions on Wireless Communications*, Vol. 22, No. 9, 6213–6226, Sep. 2023.

[21] Olivo, E. E. B., D. P. M. Osorio, H. Alves, J. C. S. S. Filho, and M. Latva-Aho, "Cognitive full-duplex decode-and-forward relaying networks with usable direct link and transmit-power constraints," *IEEE Access*, Vol. 6, 24 983–24 995, 2018.

[22] Kwon, T., S. Lim, S. Choi, and D. Hong, "Optimal duplex mode for DF relay in terms of the outage probability," *IEEE Transactions on Vehicular Technology*, Vol. 59, No. 7, 3628–3634, Sep. 2010.

[23] Shim, Y., W. Shin, and M. Vaezi, "Relay power control for in-band full-duplex decode-and-forward relay networks over static and time-varying channels," *IEEE Systems Journal*, Vol. 16, No. 1, 33–40, Mar. 2022.

[24] Shao, Y., L. Wang, and Y. Xue, "Distributed alamouti protocol for full-duplex decode-and-forward relaying networks," *IEEE Communications Letters*, Vol. 26, No. 1, 182–186, Jan. 2022.

[25] LG-Nortel, "Self interference considerations in relay node," 3GPP TDoc R1-090565, 2009.

[26] Rakhmania, A. E., H. Hudiono, U. A. Ro'isatin, and N. Hidayati, "Channel estimation methods in massive MIMO: A comparative

review of machine learning and traditional techniques," *Infocommunications Journal*, Vol. 17, No. 1, 19–31, Mar. 2025.

[27] Joann, D. and V. Rajamani, "Evaluating MIMO and massive MIMO performance with rayleigh, rician, and nakagami fading channels along with comparing half-duplex and full-duplex modes using HMR protocol," in *Innovation in MIMO Technologies, Systems, and Antennas*, IntechOpen, Dec. 2024.

[28] Lo, T. K. Y., "Maximum ratio transmission," *IEEE Transactions on Communications*, Vol. 47, No. 10, 1458–1461, Oct. 1999.

[29] Da Costa, D. B. and S. Aissa, "Dual-hop decode-and-forward relaying systems with relay selection and maximal-ratio schemes," *Electronics Letters*, Vol. 45, No. 9, 1–2, Apr. 2009.

[30] Erdogan, E. and T. Gucluoglu, "Dual-hop amplify-and-forward multi-relay maximum ratio transmission," *Journal of Communications and Networks*, Vol. 18, No. 1, 19–26, Feb. 2016.

[31] Chen, X., Z. Peng, C. Pan, H. Ren, and L.-C. Wang, "Performance analysis and power allocation of multi-pair two-way massive MIMO full-duplex DF relaying systems under Rician fading channels," *IEEE Transactions on Vehicular Technology*, Vol. 72, No. 2, 1955–1971, Feb. 2023.

[32] Tu, N. H. and K. Lee, "Performance analysis and optimization of multihop MIMO relay networks in short-packet communications," *IEEE Transactions on Wireless Communications*, Vol. 21, No. 6, 4549–4562, Jun. 2022.

[33] Gradshteyn, I. S. and I. M. Ryzhik, *Table of Integrals, Series, and Products*, 7th ed., Academic Press, San Diego, CA, USA, 2007.

[34] Wolfram Functions Site, "Gamma2 function identity," 2025, https://functions.wolfram.com/GammaBetaErf/Gamma2/26/02/01/0002/.

[35] Adamchik, V. S. and O. I. Marichev, "The algorithm for calculating integrals of hypergeometric type functions and its realization in REDUCE system," in *ISSAC'90: Proceedings of the International Symposium on Symbolic and Algebraic Computation*, 212–224, 1990.

[36] Wolfram Functions Site, "Meijerg function identity," 2025, https://functions.wolfram.com/HypergeometricFunctions/MeijerG/21/02/02/0001/.